Journal of Environmental Radioactivity 255 (2022) 107016

Contents lists available at ScienceDirect

Journal of Environmental Radioactivity

journal homepage: www.elsevier.com/locate/jenvrad

Westerly drives long-distance transport of radionuclides from nuclear events to glaciers in the Third Pole

Deji[a,*], Tandong Yao[a,b], Lonnie G. Thompson[c,d], Mary E. Davis[c], Baiqing Xu[a,b], Guangjian Wu[a,b], Sujie Liang[e], Huabiao Zhao[a,b], Meilin Zhu[f], Chao You[g]

[a] *Key Laboratory of Tibetan Environmental Changes and Land Surface Processes, Institute of Tibetan Plateau Research, Chinese Academy of Sciences (CAS), Beijing, 100101, China*
[b] *Chinese Academy of Sciences (CAS) Center for Excellence in Tibetan Plateau Earth Sciences, Beijing, 100101, China*
[c] *Byrd Polar and Climate Research Center, The Ohio State University, Columbus, OH, 43210, USA*
[d] *School of Earth Sciences, The Ohio State University, Columbus, OH, 43210, USA*
[e] *Tianjin Climate Center, Tianjin, 300074, China*
[f] *Center for the Pan-Third Pole Environment, Lanzhou University, Lanzhou, 730000, China*
[g] *College of Environment and Ecology, Chongqing University, 400044, Chongqing, China*

A R T I C L E I N F O

Keywords:
Third pole
Ice core records
Nuclear events
Radionuclides
Westerly
Water vapor divergence and convergence

A B S T R A C T

Major nuclear bomb tests and nuclear power plant incidents release large amounts of radionuclides. This study investigates beta (β) activities of radionuclides from four ice cores in the Third Pole (TP) to understand the transport routes and related atmospheric processes affecting the radionuclides deposition in glaciers of the region. All the ice cores show three major β activity peaks in the ice layers corresponding to 1963, 1986, and 2011. The β activity peak in the 1963 ice layer is referred to as the well-known 1962 Nuclear Bomb Test. Beta activity peaks in 1986 and 2011 ice layers from the Chernobyl and Fukushima Nuclear Incidents (CNI, FNI). Hysplit forward and backward trajectory analyses suggest that the radionuclides were transported by the westerly into the stratosphere and then to the high elevation TP glaciers. In the FNI case, the radionuclides traveled over Japan, the Pacific Ocean, Europe, and central Asia before being deposited in the TP glaciers. Investigations of the atmospheric circulation confirm that the stronger northern branch of westerly is responsible for high radionuclides during the FNI in the TP. Less precipitation with water vapor flux component divergence after the FNI also contributed to the enriched radionuclides.

1. Introduction

Nuclear events, such as atmospheric nuclear tests and nuclear power plant incidents, release radionuclides that threaten human health and wildlife survival through atmospheric and oceanic circulation on a hemispheric scale and even global scale (Masson et al., 2011; Bu et al., 2015). Radionuclides deposited in glaciers are transported through atmospheric circulations. There are three sources of radionuclides recorded in glaciers: 1) the geogenic source including the ^{235}U, ^{232}Th, ^{40}K, and the family of ^{238}U series like the ^{222}Rn and its decay product of ^{210}Pb; 2) the cosmic source including the atmospheric constituents or extraterrestrial material accreted by the Earth, such as ^{7}Be, ^{10}Be, ^{14}C, ^{26}Al, $^{32,33}P$, and ^{32}Si; 3) the anthropogenic source mainly arising from human activities, such as nuclear power facilities, reprocessing plants, loss of radiation sources, detonation and loss of nuclear weapons, and laboratory accidents (Mabit et al., 2012; Szymczak, 2012).

Among them, the anthropogenic radionuclides, especially the ^{131}I and ^{137}Cs, released by the nuclear events have been raised with great attention due to their high concentrations and health risk (Tang et al., 2021). Generally, the artificial radionuclides (e.g., ^{137}Cs ^{134}Cs, ^{131}I, ^{90}Sr, ^{60}Co) released from nuclear events emitted beta (β) rays during their decay (Pröhl et al., 2012). As a fission product, the β decay results in changes of both valence and ionic size (Gray, 1982). Thus, after long distances traveled in the air, the β radionuclides are deposited in glaciers by snowfall through gravitational settling.

From 1945 to 1980, the United States (US) and the former Soviet Union (FSU) conducted atmospheric Nuclear Bomb Tests (NBT). There were 85 tests conducted during the period 1957–1962, which released a

* Corresponding author.
E-mail address: deji@itpcas.ac.cn (Deji).

https://doi.org/10.1016/j.jenvrad.2022.107016
Received 26 July 2022; Received in revised form 2 September 2022; Accepted 3 September 2022
Available online 29 September 2022

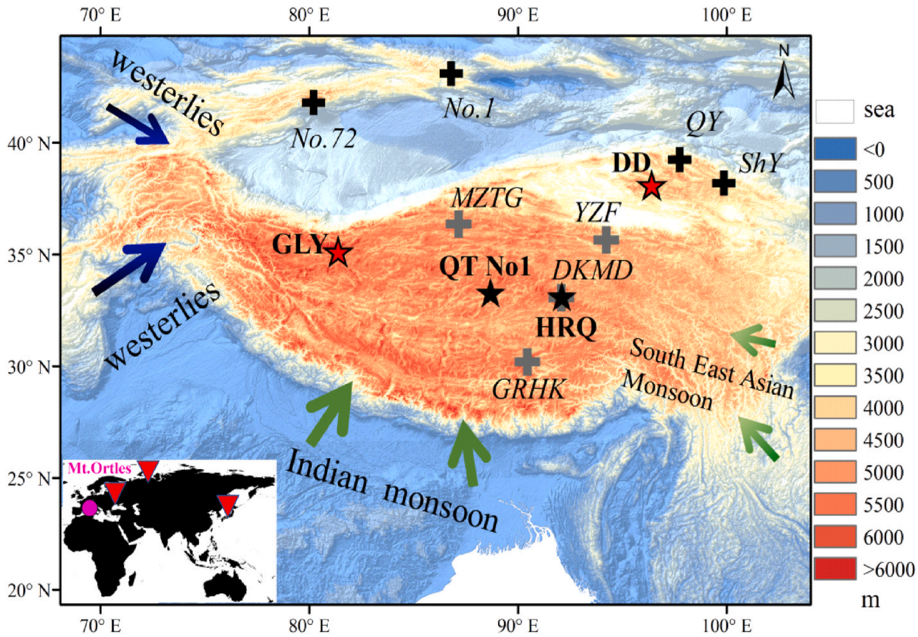

Fig. 1. Map of ice core drill sites in the TP region with dominant air masses marked by arrows. In the figure, the stars indicate the ice core drill sites discussed in this study with red stars from this study and black stars from other studies. The QT No1 ice core is referenced from Shao et al. (2020), and the HRQ ice core is referenced from Wang et al. (2021); the grey cross and black cross denote the glaciers in which the radionuclides from the Fukushima incident were identified (Wang et al., 2015, 2020). The Mt Ortles in the Italian Alps (Purple dot, referenced from Gabrielli et al., 2016) and the Fukushima, Chernobyl, and the Nuclear Bomb Test (Red triangle) are shown in the lower-left insert map. The details of each ice core (i. e., locations, altitude, drill year, etc.) are listed in Table 1. (For interpretation of the references to colour in this figure legend, the reader is referred to the Web version of this article.)

total yield of 239.6 Mt (Megatons TNT equivalents) distributed as local (~0.1%), tropospheric (~7%), and stratospheric (~93%) fallout (Wendel et al., 2013). The largest atmospheric NBT by the FSU was conducted in 1962 with a total yield of 132.7 Mt (Khalturin et al., 2005). After that, the US and the FSU signed the Partial Test Ban Treaty, a treaty stipulating a ban on NBT in all global environments (except for the underground) to prevent the dispersion of nuclear fallout and limit environmental risks. However, the construction of nuclear power plants has continued to meet economic development needs. Although technical advances have substantially reduced the environmental risks from nuclear facilities, human fallibility and natural disasters remain potential hazards (Lelieveld et al., 2012). The Ukraine Chernobyl Nuclear Incident (CNI) on 26 April 1986 released total radionuclides of 5.2×10^{18}Bq into the atmosphere, and the Fukushima Nuclear Incident (FNI) on 11 March 2011 released about 63×10^{17}Bq of radionuclides (Kortov and Ustyantsev, 2013).

With an average elevation above 4000 m.a.s.l, the Third Pole region (TP), the Tibetan Plateau and its surroundings, contains the largest number of glaciers outside Antarctica and Arctic (Yao et al., 2012). Snow continuously falls on these glaciers associated with dust and other atmospheric impurities, including radionuclides, thus incorporated into the ice with time and preserved within glaciers. Measurement of radionuclides in ice cores from known events provides a way to calibrate the time series of a climate record from ice cores and verify the pollutant diffusion by atmospheric processes with the peaks of the β radionuclides from the nuclear events.

The β activity peak of the most intensive nuclear test in 1962 performed by the FSU has been detected in glaciers and identified in the ice layer corresponding to 1963 in the Northern Hemisphere (Bautista et al., 2018) and 1964 in the Southern Hemisphere (Goursaud et al., 2017). The other two major β activity peaks detected from the glaciers all over the world are the 1986 CNI and the 2011 FNI (e.g., Haeberli et al., 1988; Di Stefano et al., 2019).

Although the β activity in ice cores is traditionally used as a chronological tool, the available β activity records in TP ice cores allow us to depict the β activity radionuclides profile of the TP glaciers and understand how the radionuclides were transported to the TP and how atmospheric circulation was driving the transport process. In this study, we examine β activity records from four high elevation ice cores across the TP and one Alps ice core to reconstruct an overall picture of the geographical dispersion of the radionuclides of the three most critical nuclear events. The Hysplit forward and backward trajectory models were used to examine the transport routes of the radionuclides from their sources to the deposition sites on the TP. The atmospheric circulation processes transporting the radionuclides are investigated by diagnosing the wind field, water vapor flux components from NCEP/NCAR reanalysis data, and observed ground precipitation from the National Meteorological Information Center (NMIC) of China Meteorological Administration (CMA) and reanalysis precipitation data from the Global Precipitation Climatology Project (GPCP), which allows us to identify the drivers of different β radionuclides from the origins of the nuclear events to the TP.

2. Materials and methods

Fig. 1 shows the drill sites of the four TP ice cores and Mt Ortles ice core (Gabrielli et al., 2016) in this study. The identification of each ice core is provided in Table 1. The ice cores were transported frozen to a cold room maintained at < −20 °C. Ice core samples with a weight between 260 and 740 g were prepared from the upper parts of the ice cores. Table S1 listed the β activity with depth for each ice core in the supplemental information. As shown in Table S1, samples for the β

Table 1
The identification of ice core drilling sites of four TP ice cores and Mt Ortles ice core.

Ice Core	Longitude (E)	Latitude (N)	Altitude (m.a.s.l)	Drill year	Drill Depth (m)	Reference
Dunde (DD)	96°24.6′	38°6.6′	5320	2016	132	This study
Guliya(GLY)	81°22.8′	35°7.8′	6200	2015	19.21	This study
Qiangtang No1(QT No 1)	88°41.4′	33°18′	5890	2014	109	Shao et al. (2020)
Hariqin (HRQ)	92°6′	33°78′	5664	2015	146.25	Wang et al. (2021)
Mt Ortles	10°32.58′	46°30.42′	3859	2011	74.88	Gabrielli et al. (2016)

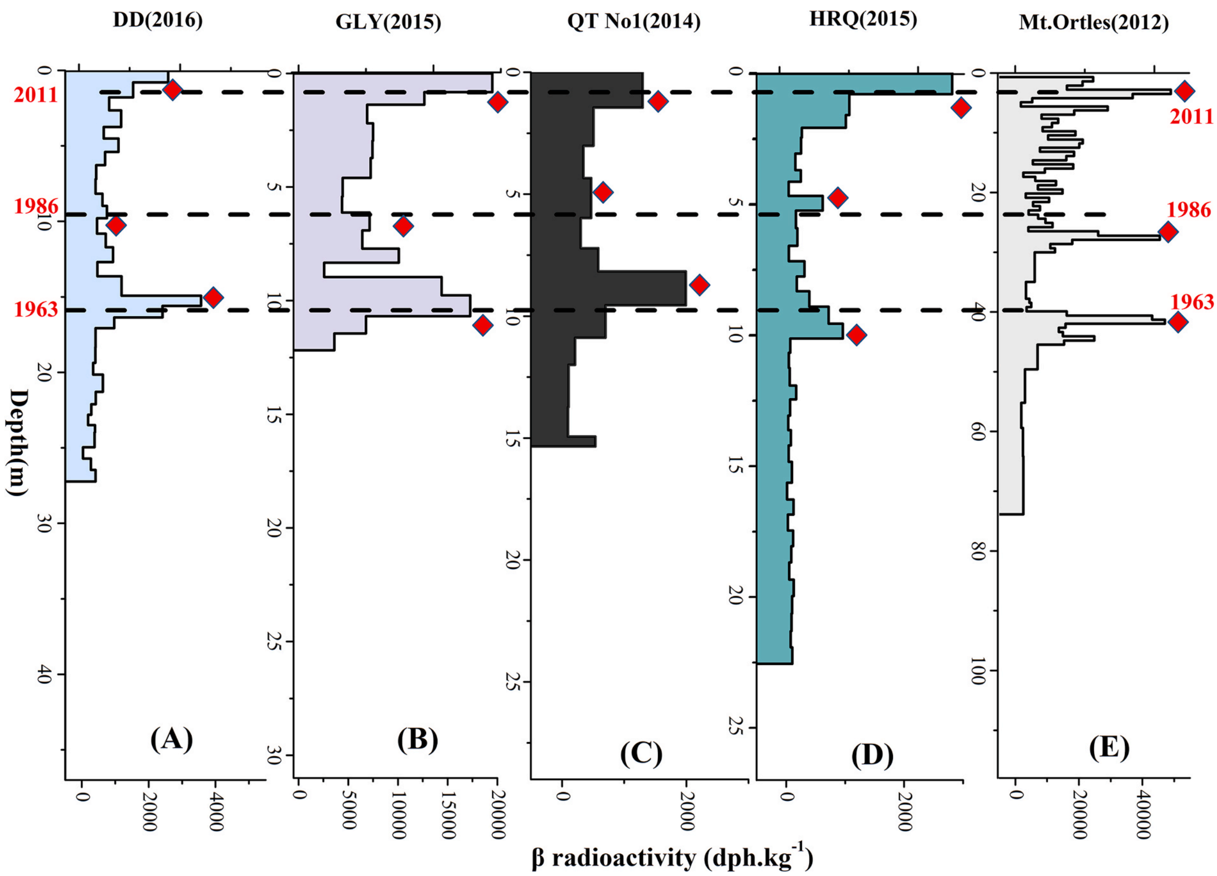

Fig. 2. Specific total β activity recorded in four TP ice cores, **(A)** Dunde, **(B)** Guliya, **(C)** Hariqin, **(D)** Qiangtang No1, and the Alpine **(E)** Mt Ortles ice core. The three β activity peaks marked by diamonds and joined by dashed lines correspond to the Fukushima nuclear incident in 2011, the Chernobyl nuclear incident in 1986, and the nuclear bomb test in 1962. Shaded plots indicate the continuous β activity analyses. Ice cores are identified by abbreviations which are defined in Table 1.

activity analysis were divided into 31, 16, 31, 11, and 6 layers for the DD, GLY, HRQ, QT No1, and Mt Ortles ice cores, respectively. Samples were melted at room temperature and then mixed with 4 mol/ml hydrochloric acid (HCl) until reaching a pH value of 2 to prevents hydrolysis and any sorption of radionuclides on the container walls and attach onto the membrane. The solution was filtered at least three times (to ensure absorption) through MN616 LSA-50 cation and MN 616 LSB-50 anion membranes. The membranes were marked and dried on aluminum foil at room temperature. The β activity was measured by the Mini 20Alpha-Beta Multidetector (French Eurisys Measures Corporation) with a detection limit of 0.03dpm (disintegration per minute).

The instrument was run for 72 h to reach a stable state at first. Then the background β activity and detector efficiency were measured by a blank sample with no contamination indicated. The background of the GLY, QT No1, and DD ice core is 0.03–0.2, 0.03–0.34, and 0.03–0.28, which are well below the actual value of β activity. Finally, each sample's β activity (dph/kg, disintegration per hour in the 1-kg sample) was measured on a Mini 20Alpha-Beta Multidetector, and the final β activity is calculated as:

$$\beta = \frac{\beta_{\text{sample}} - \beta_{\text{background}}}{\mathrm{M} * \mathrm{E}} * 60$$

where β_{sample} is the β activity measurements of ice core samples (dpm); $\beta_{\text{background}}$ is the β activity measurements of the blank sample (dpm); M is the sample's weight (kg, kilogram); E is the efficiency, which is determined using certified known alpha and beta sources.

The depth-age developments of the four ice cores are provided in Fig. S1. The three β peaks correspond to the annual time series that is based primarily on the seasonal variations of $\delta^{18}O$ in each core. The QT. No1 and HRQ have been documented in Shao et al. (2020) and Wang et al. (2021). The GLY ice core was analyzed at the Institute of Tibetan Plateau Research, Chinese Academy of Sciences (ITPCAS) as part of a cooperative program with the Byrd Polar Climate Research Center (BPCRC) at The Ohio State University. The β activity and $\delta^{18}O$ from the BPCRC ice core have been presented in Thompson et al. (2018). We show the β activity record from the part of the ITPCAS ice core for the first time in this study.

The three β activity peaks in the Mt Ortles ice core and its depth-age development were reported by Gabrielli et al. (2016).

3. Results and discussion

3.1. Beta radionuclides in Third Pole ice cores

Fig. 2 shows the specific total β activity profiles from the four TP ice cores and the Alpine Mt Ortles ice core (Gabrielli et al., 2016). The value of each peak and its factor over the background (i.e., excluding the three β peaks) are listed in Table 1. Here, as aforementioned, the $\delta^{18}O$-based time series and the β activity levels in all the ice cores are mutually supportive, confirming that the three β activity peaks represent the FNI in 2011, the CNI in 1986, and the NBT in 1962. These peaks are traditionally used for calibrating ice core time series since they represent the exact absolute year of either nuclear tests or nuclear incidents. Note that the β activity is an activity for the day of the analysis year (2015 for DD, 2016 for GLY, 2015 for HRQ, 2014 for QT No1, and 2016 for Mt Ortles) and does not take into account the decline due to the half-life.

As shown in Fig. 1, the β activity peak at the top of the GLY, HRQ, and Mt Ortles ice cores are the most pronounced. This peak corresponds to the FNI in 2011, which was extensively detected throughout the Northern Hemisphere, including eight snow pit samples from TP glaciers

Table 2
The value of the β activity peaks corresponding to the 2011 Fukushima and the 1986 Chernobyl nuclear incidents and the 1962 nuclear bomb test (which peaked in 1963 in ice core records), respectively, in the four TP ice cores and Mt Ortles ice core. The factors of each peak over its background level (the average β activity value without three β activity peak values) for each event are shown next to the columns of each β activity peak value.

Ice Core Site	2011 (dph kg^{-1})	Factor	1986 (dph kg^{-1})	Factor	1963 (dph kg^{-1})	Factor	Accumulation (i.e)
Dunde	2581.74	3.86	749.17	1.12	3569.14	5.33	294
Guliya	1170	2.77	604.8	1.43	1036.8	2.46	170
Qiangtang No1	2158.67	3.65	779.41	1.32	3318.69	5.62	185
Hariqin	2812.33	14.39	620.16	3.17	961.27	4.92	195
Mt Ortles	48900	4.05	45480	3.77	47040	3.89	881

in Fig. 1 (Wang et al., 2015, 2020), in the Mt Ortles in the Italian Alps (Gabrielli et al., 2016), and in the snow and ice samples from other high-elevation glaciers (e.g., Di Stefano et al., 2019). Airborne radiation from the FNI traveled through much of the hemisphere at lower (3–4 km) and higher altitudes (>5000 m) (Hsu et al., 2012), also comparable to the elevation of the ice core drilling sites in this study (5320–6200 m, Table 1). These records imply that atmospheric circulation might be responsible for transporting the radionuclides from the FNI to the high elevation glaciers in the Northern Hemisphere (Masson et al., 2011).

A less pronounced β activity peak in the ice layer underneath the 2011 FNI ice layer of the TP ice cores and Mt Ortles ice core corresponds to the CNI in 1986, which has been extensively reported worldwide (e.g., Ambach et al., 1987; Pinglot et al., 1994; Haeberli et al., 1988; Tian et al., 2006; Hou et al., 2018). The uniformity of the results from different studies confirms the widespread deposition of radionuclides from the CNI to the high-elevation glaciers in the Northern Hemisphere. Not only is the overall intensity lower, but also the average value of each β peak and its ratio to its respective background are lower (Table 2).

All cores show noticeable increases in β activity in the ice layer corresponding to 1963, a consequence of the former Soviet NBT program in 1962. Between 24 September 1957 and 25 December 1962, 85 atmospheric nuclear tests with a total yield of 239.6 Mt were carried out at Novaya Zemlya Test Site, including 2 tests with a yield of 4.5 Mt in 1957, 24 tests with a yield of 16.2 Mt in 1958, 24 tests with a yield of 86.2 Mt in 1961, and 35 tests with a yield of 132.7 Mt in 1962 (Khalturin et al., 2005). Of all the nuclear tests in different years, 1962 is the year with the largest radionuclides releases. The highly remarkable β activity peak in 1963 was observed in all the ice cores from middle and high latitude glaciers (e.g., Thompson et al., 2018; Bautista et al., 2018; Goursaud et al., 2017). The β activity corresponding to the 1962 NBT that occurred in 1963 is the most distinct in the DD and QT No1 records.

The peak of β radioactivity appeared at different depths in different glaciers, depending on glacier accumulations. Based on the depth corresponding to the 1963 β peak, we calculated the annually-averaged accumulation (ice equivalent) of each ice core site as shown in Table 2. The annually-averaged accumulation is the highest in the DD, moderate in the GLY and QT No1, and lowest in the HRQ. The different accumulations have resulted from different regional precipitations

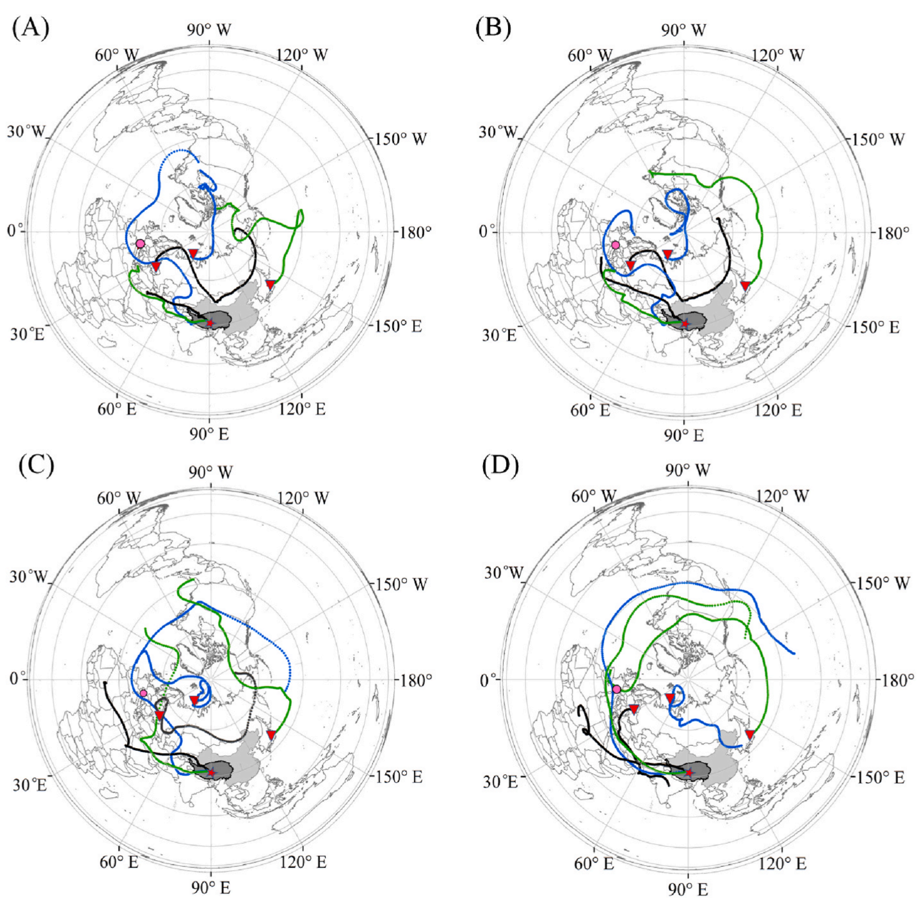

Fig. 3. Forward trajectories for the 2011 Fukushima nuclear incident (green lines), the 1986 Chernobyl nuclear incident (black lines), and the 1962 Nuclear bomb test (blue lines), along with the backward trajectory for the QT No1 ice core site for the heights at **(A)** 1500 m above ground level (AGL), **(B)** 2000m AGL, **(C)** 3000 m AGL, and **(D)** 4500 m AGL. The trajectories are determined using the HYSPLIT model (https://ready.arl.noaa.gov/archives.php) with global archive data. The shaded region indicates the TP region with the QT No1, Mt Ortles ice core, and each event site marked by a purple dot, red star, and red triangles, respectively. (For interpretation of the references to colour in this figure legend, the reader is referred to the Web version of this article.)

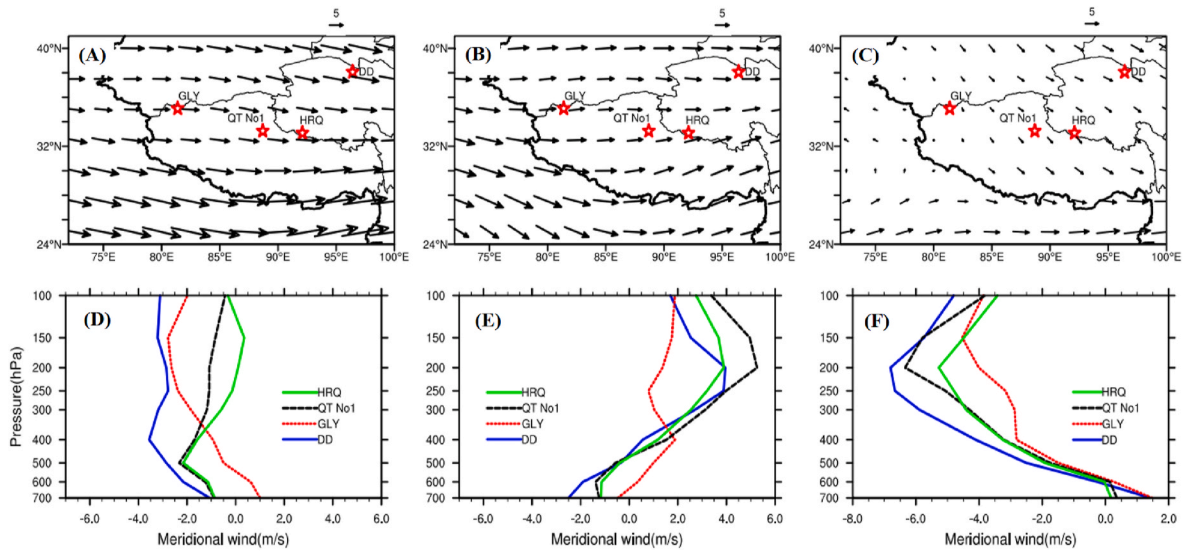

Fig. 4. Spatial patterns of the wind field (m/s, arrows) averaged at 300-700 hPa over the TP after the **(A)** Fukushima nuclear incident, **(B)** Chernobyl nuclear incident, and **(C)** the difference between 2011 and 1986 and the vertical profile of the meridional wind between 700 and 100 hPa after the **(D)** Fukushima nuclear incident, **(E)** Chernobyl nuclear incident, and **(F)** the difference between 2011 and 1986. All data are calculated for two months after each nuclear test or incident, from 11 March 2011 to 11 May 2011 after the 2011 Fukushima nuclear incident and from 26 April 1986 to 26 June 1986 after the 1986 Chernobyl nuclear incident. The data of meridional wind in Fig. 4d–f is averaged at the neighboring four points (square) of gridded data. Red stars mark the ice core drill sites in figure (Fig. 4A–C) with abbreviations defined as Fig. 1. The wind fields are from the NCEP/NCAR reanalysis data set (http://www.esrl.noaa.gov/psd/data.ncep.reanalysis.derived.html). (For interpretation of the references to colour in this figure legend, the reader is referred to the Web version of this article.)

caused by large-scale atmospheric circulation systems of the TP region (Yao et al., 2012).

3.2. Possible transportation routes of beta radionuclides from nuclear events

Forward and backward trajectories (Tositti et al., 2012) were used to reconstruct possible radionuclides transport from the three events sites to the four TP glaciers, based on the NOAA–ARL (National Oceanic and Atmospheric Administration Air Resources Laboratory) 3D kinematic HYSPLIT (Hybrid Single-Particle Lagrangian Integrated Trajectory Model) trajectory model (Stein et al., 2015). Global reanalysis data are from NCEP (National Weather Service's National Center for Environmental Prediction) (Kalnay et al., 1996). Previous studies have detected the arriving time of the radionuclides at different places after the FNI. The radionuclides anomalies from the FNI were measured on 15 March in the US, on 16 March in the North American continent, on 23 March in northwestern Europe, on 26 March in Mongolia and China (Tang et al., 2021), and on 3 April in Belarus (Masson et al., 2011). A study on TP snow pit samples suggests that the radionuclides deposited on TP glaciers approximately 20 days after the FNI (Wang et al., 2015). Based on the study, the period from 11 March to 23 March is used for our forward trajectory analysis, while the period from 23 March to 1 April 2011 is used for the backward trajectory analysis in the case of the FNI. For the CNI case, Steinhauser et al. (2014) found that after the initial peak release, further releases of radionuclides occurred over 10 days due to the graphite fire. This assumes continuous radionuclides over 10 days from the CNI. We, therefore, used the period from 26 April to 8 May in 1986 for both the forward and backward trajectory analyses in the case of the CNI. The period from 1 January to 13 January in 1963 is used for the backward trajectory of the NBT around Novaya Zemlya and 18 December to 31 December in 1962 is used for the forward trajectory. We calculated forward and backward trajectories at the heights 1500 m, 2000m, 3000 m, and 4500 m above ground level (AGL) between each event site and ice core site. The QT No1 ice core is used as the representative TP target point since it is located in the center of the four TP ice core sites (Fig. 3).

As shown in Fig. 3, the backward trajectory from the QT No 1 site is linked with the forward trajectory from the origins of NBT at the height of 1500 m AGL (Fig. 3A), indicating that the radionuclides-bearing aerosols after the NBT might be transported through the atmospheric boundary layer. The backward and forward trajectories were not linked to each other at the height of 1500 m and 2000m AGL (Fig. 3A and B) for FNI and CNI, while they were linked at the height of 3000 m AGL for the CNI and NBT (Fig. 3C). The height of 4500 m AGL is a favorable transport route for radionuclides from the origins of FNI and CNI to the QT No1 ice core (Fig. 3D). In the case of the FNI period, the forward trajectory at 4500 m AGL traveled over Japan, the Pacific Ocean, Canada, Arctic Ocean, Europe, France through the Mt Ortles, and Central Asia, while the backward trajectory from the QT No1 traveled over the Iran, Mediterranean, Netherland, Arctic Ocean, America, and the Pacific Ocean where it met with the forward trajectory. It is reasonable that the stratospheric and tropospheric intrusions transported the radionuclides from all three events, which were carried by the prevailing westerly. The upper stratospheric air mass will mix with the local tropospheric air mass bringing radionuclides and transporting the radionuclides to ice core sites. Such high-velocity movement of radioactive contamination through prevailing westerly indicates the quickly spread out of nuclear risk worldwide.

Previous studies suggest that the nuclear incidents and nuclear bomb tests injected radionuclides into the stratosphere, and transported them on regional to global scales before deposition (e.g., Aoyama, 1988; Hirose and Povinec, 2015; Malakhov and Pudovkina, 1970). The radionuclides from the FNI were firstly ejected into a high tropospheric plume and then transported around the NH (Mészáros et al., 2016). The radionuclides discharged from the FNI have been recently detected in several regions of China (Shi et al., 2014) and from the NBT and CNI in an extensive range of literature and various samples (e.g., Kortov and Ustyantsev, 2013; Steinhauser et al., 2014). Our ice core results further indicate long-range radionuclides risks from the mid-and low-troposphere transport from the recent FNI and the previous CNI and NBT in the region.

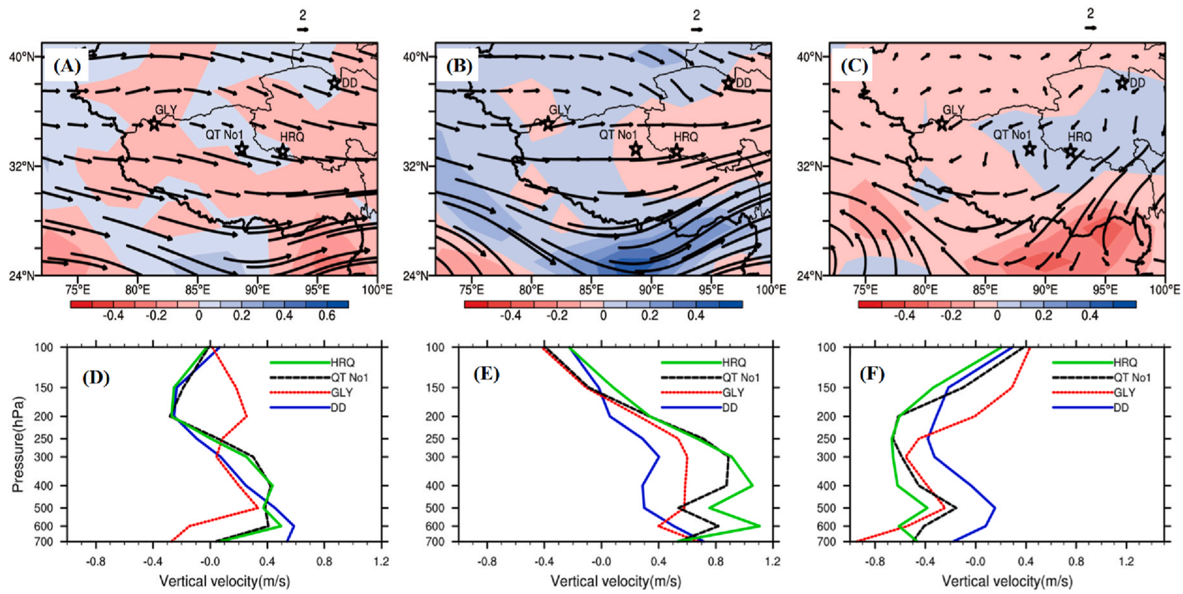

Fig. 5. Spatial patterns of vertically integrated mass-weighted water vapor flux component in the atmosphere column averaged at 300-700 hPa after the **(A)** Fukushima nuclear incident, **(B)** Chernobyl nuclear incident, and **(C)** the difference between 2011 and 1986, and the vertical profile of vertical velocity in the atmosphere column between 700 and 100 hPa after the **(D)** Fukushima nuclear incident, **(E)** Chernobyl nuclear incident, and **(F)** the difference between 2011 and 1986. The arrows in Fig. 5a–c shows the integrated mass-weighted water vapor flux components and the shading indicates the integrated divergence of water vapor flux. All data are calculated for two months after each nuclear incident, which is from 11 March 2011 to 11 May 2011 for the 2011 FNI and from 26 April 1986 to 26 June 1986 for the 1986 CNI. The vertical velocity data in Fig. 5D–F is averaged at the neighboring four points (square) of gridded data. Black stars in Fig. 5A–C mark the ice core drill sites with abbreviations defined in Fig. 1. The mean daily air temperature, pressure at the surface, relativity, and vertical velocity are downloaded from http://www.psl.noaa.gov/data/gridded/data.ncep.reanalysis.html.

3.3. Factors affecting the transport of beta radionuclides after the fukushima and chernobyl incidents

As mentioned in section 3.1, the radionuclides in the TP and Alps ice core records demonstrate that the radionuclides from the three nuclear events are preserved in high-elevation glaciers throughout Eurasia. The NBT released radionuclides are still significant because of their huge releases, which agree well with the largest peak recorded in the TP ice cores and Mt Ortles ice core in this study. The deposition processes of the FNI and CNI incidents are different in different regions worldwide. Previous comparison studies indicate that the CNI has released larger radionuclides into the atmosphere than the FNI (Lelieveld et al., 2012; Steinhauser et al., 2014). Our results from four TP ice cores showed that the β activity of radionuclides from the FNI is substantially higher than that of the CNI. Despite lesser levels compared to the TP ice core, the Mt Ortles ice core also showed 3420 higher β activities in 2011 FNI than in 1986 CNI. This difference is caused by the complexity of the atmospheric circulation systems governing the dispersion and meteorological conditions of the region (Qiao et al., 2011; Bu et al., 2015). The radionuclides from atmospheric nuclear tests and nuclear power plant incidents follow the prevailing westerly wind directions and strength, which dominate different transportation routes (Wendel et al., 2013; Haeberli et al., 1988; Huh et al., 2012). We, therefore, looked for the atmospheric circulation systems and meteorological conditions for the targeted TP region to understand the transport processes of the radionuclides deposition from the stratosphere to the glaciers on the TP.

Fig. 4 illustrates the regional wind field averaging 300-700 hPa over the TP in two months after each nuclear incident, from 11 March 2011 to 11 May 2011 for the FNI and from 26 April 1986 to 26 June 1986 for the CNI. The TP region is subject to the competing influences of two large-scale atmospheric circulation systems: the continental westerly during the winter and spring and the Indian monsoon in summer (Yao et al., 2013). It is clear from Fig. 4A and B that the westerly winds prevailing over the TP from 11 March 2011 to 11 May 2011, after the FNI, were much stronger than that on 26 April 1986 to 26 June 1986, after the CNI. The TP divides the westerly into the northern branch and southern branch at around 35°N. When the northern branch of westerly (northern westerly) is very strong, the wind speed of the southern branch of westerly (southern westerly) is weak, which is the case in 2011 after the FNI (Fig. 4A). When the northern westerly is weak, then the wind speed of the southern westerly is strong, which is the case in 1986 after the CNI (Fig. 4B). The difference in wind fields between 2011 and 1986 also indicates stronger northern westerly winds after the FNI than after the CNI (Fig. 4C). As shown in Fig. 4D–F, the vertical profile of the meridional wind between 700 and 100 hPa over each TP ice core site is averaged by the neighboring four points (square) of gridded data located at the negative phase after the FNI while it is positive after the CNI (Fig. 4D–F), confirming the northern westerly prevails after the FNI and the southern westerly combining with the Indian Monsoon dominance after the CNI. The spatial pattern of the regional wind field and the vertical profile of the meridional wind over Mt Ortles site indicate that the westerly circulation is stronger after the 2011 FNI and weaker after the 1986 CNI (Fig. S2). Thus, we suggest that the stronger westerly, particularly the stronger northern westerly prevailing over TP, is responsible for driving the high radionuclides deposition after the FNI in the TP glaciers. Due to the similar vertical profile of zonal winds at 700-100 hPa atm pressure on each TP ice core site and Mt Ortles ice core site between the two incident periods (Fig. S3), the radionuclides were possibly independent of zonal winds.

We have investigated the water vapor transport by analyzing the vertically integrated mass-weighted water vapor flux component and the divergence of water vapor flux in the atmosphere column at 300-700 hPa based on reanalysis data. The result shows that the TP ice core sites are located at the divergence zone after the 2011 FNI and the convergence zone after the 1986 CNI (Fig. 5A–C). The negative phase of the vertical wind velocity profile at 700-100 hPa after the 2011 FNI suggests the descending motion, while the positive one after the 1986 CNI suggests the ascending motion over the TP ice core (Fig. 5D–F) and Mt Ortles ice core sites (Fig. S4). It means that the divergence with descending process transported more radionuclides after the FNI, while

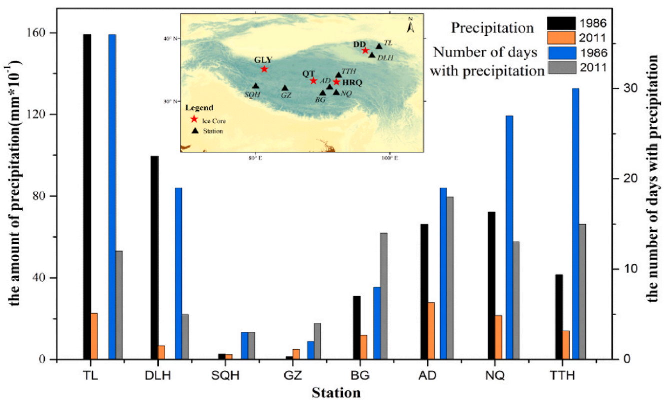

Fig. 6. The precipitation and the number of days with precipitation from eight meteorological stations in two months after each incident. The data are calculated from 11 March 2011 to 11 May 2011 for the 2011 Fukushima incident and from 26 April 1986 to 26 June 1986 for the 1986 Chernobyl incident. The spatial distribution of eight meteorological stations is shown in the top insert map (black triangles) with their neighboring ice cores (red asterisks). The identification and meteorological conditions on each station are listed in Table S2. The data on daily precipitation is from the National Meteorological Information Center (NMIC) of China Meteorological Administration (CMA). (For interpretation of the references to colour in this figure legend, the reader is referred to the Web version of this article.)

the convergence with ascending process transported less radionuclide after the CNI.

Based on the daily observation data of the neighboring eight stations of TP ice core sites and Global Precipitation Climatology Project (GPCP) reanalysis data, we have further investigated the precipitation two months after the FNI (from 11 March 2011 to 11 May 2011), late spring season, and two months after the CNI (from 26 April 1986 to 26 June 1986), early summer season (Fig. 6 and Fig. S5). The results show that the amount of precipitation and the number of days with precipitation two months after the FNI are generally less than those two months after the CNI. The radionuclides depositions in the TP glaciers were enriched due to less precipitation after the FNI and diluted due to more precipitation after the CNI.

4. Conclusions

Ice cores in the Third Pole region allow us to reconstruct the history of radionuclides deposition from nuclear events and understand their atmospheric processes. Three distinct β activity peaks were identified as the 2011 Fukushima Nuclear Incident (FNI), 1986 Chernobyl Nuclear Incident (CNI), and 1962 Nuclear Bomb Test in the four TP ice cores and the Mt Ortles ice core. The forward and backward trajectory analyses show that the upper-level westerly is instrumental in transporting radionuclides of the three nuclear events to the TP glaciers. The stronger westerly, particularly the stronger northern branch of the westerly, brought more radionuclides to the glaciers in the TP after the 2011 FNI. The weak southern branch of the westerly associated with the Indian monsoon resulted in less transportation of radionuclides and low deposition in the TP glaciers after the 1986 CNI. The divergence of water vapor flux component with descending motion process and less precipitation after the FNI also contributed to the enriched radionuclides in ice core records.

Author contributions

Deji: Writing-original draft, Validation, Formal analysis **Tandong Yao**: Conceptualization, Writing-Reviewing and Editing, Supervision **Lonnie G. THOMPSON and Mary E. DAVIS**: Conceptualization, Writing-Reviewing **Baiqing XU, Guangjian WU, Huabiao ZHAO, Sujie LIANG, Meilin ZHU**, and **Chao YOU**: Resources, Writing-Reviewing and Editing. All authors made substantial contributions to discussions of the manuscript.

Declaration of competing interest

The authors declare that they have no known competing financial interests or personal relationships that could have appeared to influence the work reported in this paper.

Data availability

Data will be made available on request.

Acknowledgments

This work is supported by the “Key Research Programs in Frontier Sciences” of the Chinese Academy of Sciences (QYZDY-SSWDQC003), “The second Comprehensive Scientific Expedition on Tibetan Plateau (2019QZKK0208)”, “International Partnership Program” of CAS (131C11KYSB20160061), the National Science Foundation Paleo Perspectives on Climate Change (1502919), and the National Natural Science Foundation of China (42101133, 41971092). Special thanks are extended to D. M. QU, Y. Y. Shi for experimental support and to Z.L. Yu, G.M. Wu, X.J. Zou, R. Zhang, Z. Liu, J.J. Sun, X. Zou, H.W, Dong, S.H. Wang, S.E. Porter, E. Beaudon, W.T. Hu, J.B. Zong, and A.B. Wilson for their technical support.

Appendix A. Supplementary data

Supplementary data to this article can be found online at https://doi.org/10.1016/j.jenvrad.2022.107016.

References

Ambach, W., Rehwald, W., Blumthaler, M., Eisner, H., 1987. Chernobyl fallout on Alpine Glaciers: a new reference horizon for dating. Trans. Am. Geophys. Union 68 (45). https://doi.org/10.1029/eo068i045p01577-01, 1577-1577.

Aoyama, Michio, 1988. Evidence of stratospheric fallout of caesium isotopes from the Chernobyl accident. Geophys. Res. Lett. 15 (4), 327–330. https://doi.org/10.1029/GL015i004p00327.

Bautista, A.T., Miyake, Y., Matsuzaki, H., Iizuka, Y., Horiuchi, K., 2018. High-resolution 129 I bomb peak profile in an ice core from SE-Dome site, Greenland. J. Environ. Radioact. 184, 14–21. https://doi.org/10.1016/j.jenvrad.2017.12.015.

Bu, W., Ni, Y., Guo, Q., Zheng, J., Uchida, S., 2015. Pu isotopes in soils collected downwind from Lop Nor: regional fallout vs. global fallout. Sci Rep-Uk 5. https://doi.org/10.1038/srep12262.

Di Stefano, E., Clemenza, M., Baccolo, G., Delmonte, B., Maggi, V., 2019. Cs-137 contamination in the Adamello glacier: improving the analytical method. J. Environ. Radioact. 208, 106039 https://doi.org/10.1016/j.jenvrad.2019.106039.

Gabrielli, P., Barbante, C., Bertagna, G., Berto, M., Binder, D., Carton, A., Carturan, L., Cazorzi, F., Cozzi, G., Dalla Fontana, G., Davis, M., De Blasi, F., Dinale, R., Draga, G., Dreossi, G., Festi, D., Frezzotti, M., Gabrieli, J., Galos, S.P., Ginot, P., Heidenwolf, P., Jenk, T.M., Kehrwald, N., Kenny, D., Magand, O., Mair, V., Mikhalenko, V., Lin, P.N., Oeggl, K., Piffer, G., Rinaldi, M., Schotterer, U., Schwikowski, M., Seppi, R., Spolaor, A., Stenni, B., Tonidandel, D., Uglietti, C., Zagorodnov, V., Zanoner, T., Zennaro, P., 2016. Age of the Mt. Ortles ice cores, the tyrolean iceman and glaciation of the highest summit of south tyrol since the northern hemisphere climatic optimum. Cryosphere 10, 2779–2797. https://doi.org/10.5194/tc-10-2779-2016.

Goursaud, S., Masson-Delmotte, V., Favier, V., Preunkert, S., Fily, M., Gallée, H., Jourdain, B., Legrand, M., Magand, O., Minster, B., 2017. A 60-year ice-core record of regional climate from Adélie Land, coastal Antarctica. Cryosphere 11, 343–362. https://doi.org/10.5194/tc-2016-179.

Gray, W., 1982. Fission product transmutation effects on high-level radioactive waste forms. Nature 296, 547–549. https://doi.org/10.1038/296547a0.

Haeberli, W., Gäggeler, H., Baltensperger, U., Jost, D., Schotterer, U., 1988. The signal from the Chernobyl accident in high-altitude firn areas of the Swiss Alps. Ann. Glaciol. 10, 48–51. https://doi.org/10.1017/s0260305500004158.

Hirose, K., Povinec, P.P., 2015. Sources of plutonium in the atmosphere and stratosphere-troposphere mixing. Sci Rep-Uk 5, 1–9. https://doi.org/10.1038/srep15707.

Hou, S.G., Jenk, T.M., Zhang, W.B., Wang, C.M., Wu, S.Y., Wang, Y.T., Pang, H.X., Schwikowski, M., 2018. Age ranges of the Tibetan ice cores with emphasis on the Chongce ice cores, western Kunlun Mountains. Cryosphere 12, 2341–2348. https://doi.org/10.5194/tc-12-2341-2018.

Hsu, S.C., Huh, C.A., Chan, C.Y., Lin, S.H., Lin, F.J., Liu, S.C., 2012. Hemispheric dispersion of radioactive plume laced with fission nuclides from the Fukushima nuclear event. J. Geophys. Res. 39 https://doi.org/10.1029/2011GL049986.
Huh, C.-A., Hsu, S.-C., Lin, C.-Y., 2012. Fukushima-derived fission nuclides monitored around Taiwan: free tropospheric versus boundary layer transport. Earth Planet Sci. Lett. 319, 9–14. https://doi.org/10.1016/j.epsl.2011.12.004.
Kalnay, E., Kanamitsu, M., Kistler, R., Collins, W., Deaven, D., Gandin, L., Iredell, M., Saha, S., White, G., Woollen, J., 1996. The NCEP/NCAR 40-year reanalysis project. Bull. Am. Meteorol. Soc. 77, 437–472. https://doi.org/10.1175/1520-0477(1996)077<0437:TNYRP>2.0.CO;2.
Khalturin, V.I., Rautian, T.G., Richards, P.G., Leith, W.S., 2005. A review of nuclear testing by the Soviet union at Novaya Zemlya, 1955–1990. Sci. Global Secur. 13, 1–42. https://doi.org/10.1080/08929880590961862.
Kortov, V., Ustyantsev, Y., 2013. Chernobyl accident: causes, consequences and problems of radiation measurements. Radiat. Meas. 55, 12–16. https://doi.org/10.1016/j.radmeas.2012.05.015.
Lelieveld, J., Kunkel, D., Lawrence, M.G., 2012. Global risk of radioactive fallout after major nuclear reactor accidents. Atmos. Chem. Phys. 12, 4245–4258. https://doi.org/10.5194/acp-12-4245-2012.
Mabit, L., Dornhofer, P., Martin, P., Toloza, A., Zupanc, V., 2012. Depth distribution of selected geogenic radionuclides (40 K, 226 Ra, 232 Th) and anthropogenic ^{137} Cs in an undisturbed forest soil in East Slovenia. Indian J. Pure Appl. Phys. 50, 45–48.
Malakhov, S.G., Pudovkina, I.B., 1970. Strontium 90 fallout distribution at middle latitudes of the Northern and Southern Hemispheres and its relation to precipitation. J. Geophys. Res. 75, 3623–3628. https://doi.org/10.1029/JC075i018p03623.
Masson, O., Baeza, A., Bieringer, J., Brudecki, K., Bucci, S., Cappai, M., Carvalho, F.P., Connan, O., Cosma, C., Dalheimer, A., Didier, D., Depuydt, G., De Geer, L.E., De Vismes, A., Gini, L., Groppi, F., Gudnason, K., Gurriaran, R., Hainz, D., Halldorsson, O., Hammond, D., Hanley, O., Holey, K., Homoki, Z., Ioannidou, A., Isajenko, K., Jankovic, M., Katzlberger, C., Kettunen, M., Kierepko, R., Kontro, R., Kwakman, P.J.M., Lecomte, M., Vintro, L.L., Leppanen, A.P., Lind, B., Lujaniene, G., Mc Ginnity, P., Mc Mahon, C., Mala, H., Manenti, S., Manolopoulou, M., Mattila, A., Mauring, A., Mietelski, J.W., Moller, B., Nielsen, S.P., Nikolic, J., Overwater, R.M. W., Palsson, S.E., Papastefanou, C., Penev, I., Pham, M.K., Povinec, P.P., Rameback, H., Reis, M.C., Ringer, W., Rodriguez, A., Rulik, P., Saey, P.R.J., Samsonov, V., Schlosser, C., Sgorbati, G., Silobritiene, B.V., Soderstrom, C., Sogni, R., Solier, L., Sonck, M., Steinhauser, G., Steinkopff, T., Steinmann, P., Stoulos, S., Sykora, I., Todorovic, D., Tooloutalaie, N., Tositti, L., Tschiersch, J., Ugron, A., Vagena, E., Vargas, A., Wershofen, H., Zhukova, O., 2011. Tracking of airborne radionuclides from the damaged Fukushima dai-ichi nuclear reactors by European networks. Environ. Sci. Technol. 45, 7670–7677. https://doi.org/10.1021/es2017158.
Mészáros, R., Leelőssy, Á., Kovács, T., Lagzi, I., 2016. Predictability of the dispersion of Fukushima-derived radionuclides and their homogenization in the atmosphere. Sci Rep-Uk 6, 19915. https://doi.org/10.1038/srep19915.
Pinglot, J., Pourchet, M., Lefauconnier, B., Hagen, J., Vaikmäe, R., Punning, J., Watanabe, O., Takahashi, S., Kameda, T., 1994. Natural and artificial radioactivity in the Svalbard glaciers. J. Environ. Radioact. 25, 161–176. https://doi.org/10.1016/0265-931X(94)90013-2.
Pröhl, G., Twining, J.R., Crawford, J., 2012. Radiological consequences modelling. Tropical Radioecology 281–342. https://doi.org/10.1016/b978-0-08-045016-2.00007-2.
Qiao, F., Wang, G., Zhao, W., Zhao, J., Dai, D., 2011. Predicting the spread of nuclear radiation from the damaged Fukushima nuclear power plant. Sci. Bull. 56, 1890–1896. CNKI:SUN:JXTW.0.2011-18-005.
Shao, L., Tian, L., Wu, G., Naftz, D., Cai, Z., Wang, C., et al., 2020. Dating of an alpine ice core from the interior of the Tibetan Plateau. Quat. Int. 544, 88–95. https://doi.org/10.1016/j.quaint.2020.02.030.
Shi, E., Cui, Y., Zhang, Q., Li, D., Li, X., Yao, S., Liu, M.-h., Guo, J.-q., 2014. Radioactive impact of the Fukushima nuclear accident on Shenyang in the northeast of China. J. Radiol. Prot. 34, 223. https://doi.org/10.1088/0952-4746/34/1/223.
Stein, A., Draxler, R.R., Rolph, G.D., Stunder, B.J., Cohen, M., Ngan, F., 2015. NOAA's HYSPLIT atmospheric transport and dispersion modeling system. Bull. Am. Meteorol. Soc. 96, 2059–2077. https://doi.org/10.1175/BAMS-D-14-00110.1.
Steinhauser, G., Brandl, A., Johnson, T.E., 2014. Comparison of the Chernobyl and Fukushima nuclear accidents: a review of the environmental impacts. Sci. Total Environ. 470, 800–817. https://doi.org/10.1016/j.scitotenv.2013.10.029.
Szymczak, R., 2012. Tropical Radiochemical Oceanography, *Radioact.* Radioact. Environ Elsevier, pp. 121–153.
Tang, Z., Jiang, S., Cai, J., Li, Q., Li, X., Gong, Z., 2021. Evaluating the impact of airborne radionuclides caused by the Fukushima nuclear accident on China based on global atmospheric dispersion. Prog. Nucl. Energy 139, 103869. https://doi.org/10.1016/j.pnucene.2021.103869.
Thompson, L.G., Yao, T., Davis, M.E., Mosley-Thompson, E., Wu, G., Porter, S.E., Xu, B., Lin, P.N., Wang, N., Beaudon, E., 2018. Ice core records of climate variability on the Third Pole with emphasis on the Guliya ice cap, western Kunlun Mountains. Quat. Sci. Rev. 188, 1–14. https://doi.org/10.1016/j.quascirev.2018.03.003.
Tian, L., Yao, T., Li, Z., MacClune, K., Wu, G., Xu, B., Li, Y., Lu, A., Shen, Y., 2006. Recent rapid warming trend revealed from the isotopic record in Muztagata ice core, eastern Pamirs. J. Geophys. Res. Atmos. 111, D13. https://doi.org/10.1029/2005JD006249.
Tositti, L., Brattich, E., Cinelli, G., Previti, A., Mostacci, D., 2012. Comparison of radioactivity data measured in PM10 aerosol samples at two elevated stations in northern Italy during the Fukushima event. J.Environ.Radioactiv 114, 105–112. https://doi.org/10.1016/j.jenvrad.2012.01.016.
Wang, F., Ming, J., Edwards, R., Li, Z., Wang, N., 2020. The fallout from Fukushima Daiichi nuclear accident profiles a new dating reference in ice and comparison with the Chernobyl accident. Environ. Res. Lett. 15, 084016 https://doi.org/10.1088/1748-9326/ab83a9.
Wang, M., Xu, B., Wang, H., Zhang, R., Yang, Y., Gao, S., Tang, X., Wang, N., 2021. Black carbon deposited in Hariqin glacier of the central Tibetan plateau record changes in the emission from eurasia. Environ. Pollut. 273, 115778 https://doi.org/10.1016/j.envpol.2020.115778.
Wang, N.L., Wu, X.B., Kehrwald, N., Li, Z., Li, Q.L., Jiang, X., Pu, J.C., 2015. Fukushima nuclear accident recorded in Tibetan plateau snow pits. PLoS One 10, e0116580. https://doi.org/10.1371/journal.pone.0116580.
Wendel, C.C., Fifield, L.K., Oughton, D.H., Lind, O.C., Skipperud, L., Bartnicki, J., Tims, S.G., Høibråten, S., Salbu, B., 2013. Long-range tropospheric transport of uranium and plutonium weapons fallout from Semipalatinsk nuclear test site to Norway. Environ. Int. 59, 92–102. https://doi.org/10.1016/j.envint.2013.05.017.
Yao, T., Masson-Delmotte, V., Gao, J., Yu, W., Yang, X., Risi, C., Sturm, C., Werner, M., Zhao, H., He, Y., 2013. A review of climatic controls on $\delta^{18}O$ in precipitation over the Tibetan Plateau: observations and simulations. Rev. Geophys. 51, 525–548. https://doi.org/10.1002/rog.20023.
Yao, T., Thompson, L., Yang, W., Yu, W., Gao, Y., Guo, X., Yang, X., Duan, K., Zhao, H., Xu, B., 2012. Different glacier status with atmospheric circulations in Tibetan Plateau and surroundings. Nat. Clim. Change 2, 663–667. https://doi.org/10.1038/NCLIMATE1580.